Use of fluorescence to determine the effects of cholesterol on lipid behavior in sphingomyelin liposomes and erythrocyte membranes

Brian M. Stott,* Mai P. Vu,* Chisako O. McLemore,* M. Shaun Lund,† Elizabeth Gibbons,* Taylor J. Brueseke,* Heather A. Wilson-Ashworth,† and John D. Bell[1],*

Department of Physiology and Developmental Biology,* Brigham Young University, Provo, UT 84602; and Department of Biology,† Utah Valley State College, Orem, UT 84058

Abstract The purpose of this study was to generate the equivalent of a cholesterol/temperature phase map for a biological membrane using fluorescence spectroscopy. The pseudo-phase map was created using human erythrocytes treated with various concentrations of methyl-β-cyclodextrin to remove defined amounts of cholesterol and a trio of fluorescent probes that assess different membrane properties (laurdan, diphenylhexatriene, and merocyanine 540). Parallel experiments with two-photon microscopy suggested that changes in cellular cholesterol content affected the entire membrane rather than being localized to specific macroscopic domains. The various regions of the composite erythrocyte pseudo-phase map were interpreted using analogous data acquired from multilamellar vesicles that served as simplified models of cholesterol-dependent phases. The vesicles consisted of various concentrations of cholesterol (0 to 50 mol%) with either palmitoyl sphingomyelin, 1:1 dipalmitoylphosphatidylcholine and dioleoylphosphatidylcholine, or phospholipid mixtures intended to simulate either the inner or outer leaflet of erythrocyte membranes. Four distinguishable regions were observed in sphingomyelin phase maps corresponding to the traditional solid-ordered and liquid-disordered phases and two types of liquid-ordered behavior. Physical properties were less diverse in the mixed phospholipid vesicles, as expected, based on previous studies. Erythrocytes displayed five regions of different combinations of membrane properties along the phase map. Some of the observations identified similarities between the cells and liquid-ordered behavior observed in the various types of liposomes as well as some interesting differences.—Stott, B. M., M. P. Vu, C. O. McLemore, M. S. Lund, E. Gibbons, T. J. Brueseke, H. A. Wilson-Ashworth, and J. D. Bell. **Use of fluorescence to determine the effects of cholesterol on lipid behavior in sphingomyelin liposomes and erythrocyte membranes. *J. Lipid Res.* 2008.** 49: **1202–1215.**

Supplementary key words merocyanine 540 • diphenylhexatriene • laurdan • methyl-β-cyclodextrin • two-photon microscopy • temperature

Sphingomyelin is found preferentially in the outer leaflet of plasma cell membranes (1). Accumulating evidence suggests that instead of being distributed homogeneously across the cell surface, it is enriched in complex domains called lipid rafts (2). Physically, these domains are characterized by properties that resemble the liquid-ordered phase formed by mixtures of cholesterol and saturated phospholipids (3, 4). In three-component systems consisting of unsaturated phospholipids, saturated phospholipids, and cholesterol, liquid-ordered domains form probably through preferential interactions between the sterol and saturated lipids (5). The nature of these interactions is not fully known but appears to involve a variety of forces other than the original proposal of hydrogen bonds; these include van der Waals forces, charge-pair interactions between the sphingomyelin head group and cholesterol oxygen, and relief of hydrophobic mismatches among lipid constituents in the membrane (6–8). Presumably, analogous forces are involved in the formation of biological rafts, because sphingomyelin is the principal saturated phospholipid in cell membranes (6, 9).

Techniques such as nuclear magnetic resonance spectroscopy and X-ray diffraction have been used to characterize the properties of liquid-ordered domains, i.e., lipid lateral diffusion, chain order, and geometrical dimensions and organization in phospholipid-cholesterol systems. These techniques provide excellent data unavailable from other methods for binary and ternary systems (10, 11). However, they are not useable with the complex membranes of living cells. Fluorescence spectroscopy and microscopy provide indirect information at lower resolution, but can be used in both model systems and living membranes with manageable perturbation to the bilayer. The ability of fluorescent membrane probes to resolve physical properties can be improved by making multiple measurements on

This work was supported by the National Institutes of Health, Grant GM-073997.

Manuscript received 22 October 2007 and in revised form 7 February 2008.

Published, JLR Papers in Press, February 25, 2008.
DOI 10.1194/jlr.M700479-JLR200

[1] To whom correspondence should be addressed.
e-mail: John_bell@byu

the same system with various probes that sense different properties (12, 13).

Our long-term goal is to use fluorescence spectroscopy and microscopy to characterize the effects of cholesterol on the physical properties of biological membranes. An initial step toward that end was to develop the use of multiple probes to assess properties of different thermodynamic phases in a well-characterized system. Accordingly, we have used the fluorescent probes nystatin, prodan, bispyrene, merocyanine 540 (MC540), diphenylhexatriene (DPH), and laurdan to map lipid behavior across the dipalmitoylphosphotidylcholine (DPPC)-cholesterol phase diagram (13). This report takes the next steps toward achieving our goal. First, we extend the previous efforts with laurdan, DPH, and MC540 to more relevant systems involving sphingomyelin, unsaturated phosphatidylcholine, and other lipids present in erythrocyte membranes. Then, we apply the process to explore the behavior of cholesterol in a simple biological setting, human erythrocytes treated with methyl-β-cyclodextrin (MBCD).

Laurdan detects changes in membrane phase properties through its sensitivity to the polarity of its immediate environment. It binds to phospholipid bilayers at the level of the glycerol backbones, where it senses the presence of water molecules that have penetrated to that depth (14). Bilayer water content varies as a result of changes in lipid order and causes shifts in laurdan emission spectra because of the solvent relaxation effect. Hence, the spectrum red shifts from a maximum at about 430 nm in an ordered membrane environment to about 480 nm in one that is disordered. The shifts can be quantified and measured as a parameter called the generalized polarization (GP) (14).

DPH responds to changes in physical properties of the acyl chain region of the membrane that affect its ability to rotate. Probe movement is quantified by measuring the degree to which DPH fluorescence emission is depolarized (i.e., isotropic) following excitation by polarized light. These fluorescence anisotropy measurements respond to changes in both the fluidity and order of the probe's surrounding environment. Changes in fluidity alter the rate of probe movement, whereas lipid order determines the range of possible motion.

The localized negative charge (sulfate group) of MC540 causes the probe to bind superficially to the external leaflet of bilayers. Changes in fluorescence emission of the probe provide information about lipid spacing. The wavelength of maximum emission intensity occurs at about 621 nm when the probe is bound to membranes in which the phospholipids are closely spaced. When lipids are more loosely packed and the intermolecular spacing is therefore greater, the probe displays a maximum intensity at about 585 nm with a large increase in quantum yield (15). The spectral differences observed between MC540 bound to tightly or loosely packed lipids may relate to alterations in probe orientation from a position parallel to the membrane surface to one perpendicular and immersed among lipid chains as inter-lipid spacing increases (16).

In this paper, "fluidity" of the membrane denotes the lateral and/or rotational mobility of lipids. "Order" represents the conformation of carbon–carbon bonds along the phospholipid fatty-acid chains; increased disorder reflects increased numbers of gauche conformations. "Spacing" implies the relative intermolecular distance among phospholipid heads.

MATERIALS AND METHODS

Reagents

Palmitoyl sphingomyelin (*N*-palmitoyl-D-*erythro*-sphingosylphosphorylcholine), DPPC, dioleoylphosphatidylcholine (DOPC), phosphatidylserine (porcine brain), and phosphatidylethanolamine (bovine liver) were purchased from Avanti Polar Lipids (Birmingham, AL). Cholesterol was obtained from Sigma-Aldrich (St. Louis, MO). MC540, DPH, and laurdan were acquired from Molecular Probes (Eugene, OR, now a subsidiary of Invitrogen; Carlsbad, CA). Human erythrocytes were obtained from blood samples remaining after physical exams at the Brigham Young University Student Health Center. For experiments, cells were washed and suspended in minimum basic salt solution [(MBSS) 134 mM NaCl, 6.2 mM KCL, 1.6 mM $CaCl_2$, 1.2 mM $MgCl_2$, 18 mM HEPES, 13.6 mM glucose, pH 7.4, at 37°C] at 3% of the original hematocrit (hct) as described previously (17).

Liposome preparation

To form liposomes, the indicated lipids (dissolved in chloroform) were mixed with laurdan, DPH, or MC540 to give a final probe-to-lipid ratio of 1:200. In some experiments, the fluorescent probes were equilibrated with preformed liposomes. Liposomes were prepared fresh on the day of the experiment to minimize the possibility of cholesterol oxidation. The solution was dried under a nitrogen stream. Dried lipid mixtures were hydrated in 150 mM KCl, 20 mM sodium citrate/citric acid buffer (pH 7.0) at 50°C with periodic agitation on a vortex mixer. This procedure yielded multi-lamellar vesicles.

Cholesterol extraction from erythrocytes

Washed erythrocyte samples (0.15% hct final) were incubated at 37°C for 30 min in 1 ml MBSS with or without MBCD (0.1–1.0 mM). Following incubation, cells were washed and resuspended in fresh MBSS. Laurdan or DPH was added to the cells at a final concentration of 2.5 μM, and samples were incubated for 20 min at 40°C to equilibrate the probe with cell membranes. Samples were then incubated an additional 5 min at room temperature prior to data acquisition in the fluorometer (see below). For experiments involving MC540, probe was added to cells (0.5 μM final) and incubated for 20 min at 40°C. Cells were then washed and resuspended in MBSS for experiments.

The amount of cholesterol extracted was assessed by measuring both the amount bound to MBCD as well as the amount retained in the cell membrane. Cells were treated with MBCD as described above and separated from the aqueous phase by centrifugation (1,000 *g* for 2 min). Cholesterol was isolated from MBCD in the aqueous phase by adding 900 μl chloroform to 900 μl supernatant, vortexing, removing the organic layer, and drying it under a nitrogen stream. Cell pellets were frozen in liquid nitrogen to lyse the cells. Samples were quickly thawed, and lipids were extracted with chloroform and methanol using the method of Bligh and Dyer (18). In brief, 150 μl of chilled MBSS was added to suspend the pellet, followed by 125 μl chloroform and 250 μl methanol. After vortexing the tubes for 10 s, 125 μl deionized water was added. The samples were

vortexed again and centrifuged for 30 s at 1,000 *g*. The residual organic layer was separated and dried under a nitrogen stream. Dried samples were stored at −20°C for subsequent assay of cholesterol content.

Cholesterol was assayed using the Amplex® Red kit (Invitrogen). Stock solutions of reagents were prepared and stored at −20°C. Samples were prepared by adding 50 μl of distilled water and 50 μl of Amplex® Red working solution to the dried supernatant and cell extracts. These suspensions were then incubated for 30 min at 37°C in a shaking water bath, after which 50 μl was removed and added to 1,950 μl deionized water in a quartz fluorometer sample cell. Emission spectra were collected with excitation at 560 nm and emission from 570 to 700 nm. Intensity values for experimental samples were compared with a standard curve to determine concentrations.

Fluorescence spectroscopy

Steady-state fluorescence emission spectra were obtained with a Fluoromax (Jobin Yvon; Edison, NJ) or PC-1 (ISS; Champaign, IL) photon-counting spectrofluorometer. Temperature was controlled by a circulating water bath, and sample homogeneity was maintained by continuous magnetic stirring. Bandpass (both excitation and emission) was set between 4 and 16 nm, depending on the instrument and sample intensity.

Steady-state fluorescence anisotropy measurements (DPH) were obtained in the L-format using the PC-1 fluorometer equipped with Glan-Thompson polarizers and 16 nm bandpass on both monochromators. Fluorescence intensity was measured with excitation (350 nm) and emission (452 nm) polarizers parallel to each other (both oriented at 0° from vertical) and repeated in the perpendicular configuration (excitation 0° and emission 90°). The correction factor for emission monochromator transmission efficiency was obtained from the ratio of emission intensity at 0° and 90° with the excitation polarizer oriented at 90°. Emission spectra for MC540 and laurdan were collected at wavelengths appropriate for each probe (MC540: excitation = 540 nm, emission = 550–700 nm; laurdan: excitation = 350 nm, emission = 400–600 nm) using nonpolarized light.

Liposome samples (50 μM lipid, 250 nM fluorescent probe) were equilibrated in the fluorometer at 24–25°C prior to data acquisition. After obtaining data at 24–25°C, temperature was raised by 1–3°C, the sample was reequilibrated (15 min), and fluorescence data were again acquired. The process was repeated until reaching the upper temperature of the experiment (40–48°C; see individual figures). To verify reversibility, data from the same sample were then acquired after returning the temperature to 24°C. Under the conditions used, interference from scattered light was negligible.

For erythrocytes, laurdan emission spectra, and DPH anisotropy, measurements were obtained as for liposomes every 3°C, from 21°C up to 42°C. Samples stained with MC540 were assessed first at 42°C, and the temperature was lowered progressively (3°C decrements) to 21°C. In each case, samples were equilibrated for at least 5 min after each temperature adjustment before acquiring fluorescence data. Background fluorescence (light scatter) was significant for erythrocytes and was therefore quantified and subtracted for each sample using aliquots without probe.

Analysis of fluorescence

Laurdan GP values were computed using averages of laurdan intensities at 432–438 nm and 494–506 nm as described (13, 14). For analysis of MC540 emission spectra, data were quantified as the ratio of intensities at 583–587 nm and 619–623 nm. Anisotropy (DPH) was calculated using the traditional equation (19). For erythrocytes, MC540 fluorescence at each temperature was expressed as a normalized intensity rather than a ratio, owing to the small signal size. Intensities (integrated from 560 to 600 nm) were normalized by dividing the integrated intensity at each temperature by the average intensity (all temperatures) for the same sample. The average of at least six blood samples was then scaled to the maximum and minimum as justified previously (13).

Contour plots were generated by graphing the relevant fluorescence parameter (i.e., laurdan GP, DPH anisotropy, MC540 ratio or intensity) as the Z axis, with temperature along the Y axis and cholesterol concentration on the X axis. Data were smoothed by two-dimensional nonlinear regression using arbitrary functions (e.g., exponential or polynomial functions). This was accomplished by fitting the raw data at the various cholesterol concentrations with temperature as the independent variable. The idealized values obtained from the regressions were then fit again, with cholesterol concentration as the independent variable. The optimized values from the second regression were then used to generate the plots. Plots are oriented in the figures with the Z axis perpendicular to the plane of the paper. Contour lines represent increments in the fluorescence parameter values as specified in the figure legends.

Two-photon scanning microscopy

Two-photon laurdan images were obtained at the Laboratory for Fluorescence Dynamics (University of California, Irvine) as described previously (20, 21). Laser emission was 780 or 790 nm (depending on laser stability and performance each day). For GP, dual images were collected simultaneously using a beamsplitter and interference filters (Ealing 490 and Ealing 440). Erythrocyte samples were prepared as described above for fluorescence spectroscopy. Samples were placed in thermostated microscopy dishes (Bioptechs; Butler, PA) and incubated with laurdan (250 nM final) for at least 10 min at the indicated temperature prior to image acquisition.

Images of laurdan GP were produced and analyzed using software provided by the Laboratory. Histograms displaying the number of pixels at each GP value were obtained for individual cells and also for the central region (45.9 ± 4.9% of the total cell area) of those same cells. Histograms for the perimeter of each cell were calculated by subtraction of the data representing the central region from that corresponding to the whole cell. Histograms were smoothed and normalized to the maximum signal by nonlinear regression using an arbitrary function.

RESULTS

Liposomes containing cholesterol

Laurdan emission spectra. **Figure 1A** illustrates emission spectra of laurdan in liposomes composed of 100% sphingomyelin. At 24°C, the maximum intensity was centered at about 430 nm (solid curve). As temperature was increased to 48°C, the total intensity decreased, and the maximum intensity was now centered at 470 nm (dashed curve). To quantify these spectral changes, we calculated the GP from intensity values at 435 nm and 500 nm (14). Decreased GP values indicate increased solvent relaxation, which can occur owing to penetration of the membrane by polar solvent molecules when the lipids are more disordered.

Figure 1B displays a detailed temperature profile of laurdan fluorescence in sphingomyelin liposomes. GP values decreased as temperature was raised, consistent with more

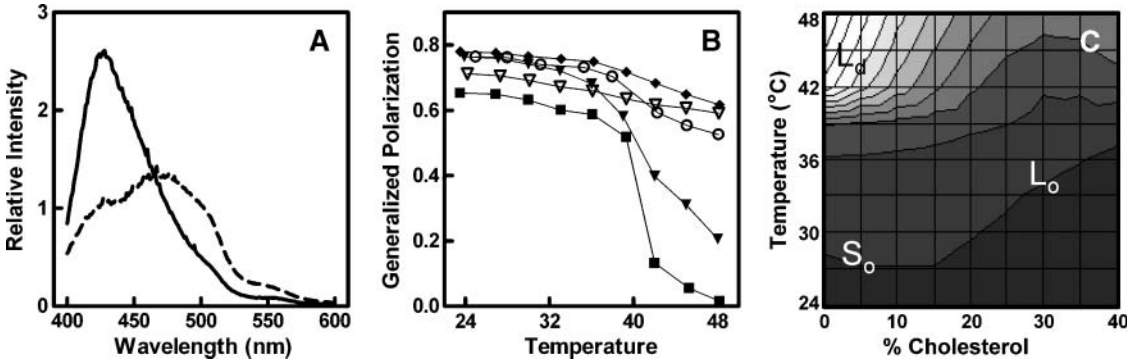

Fig. 1. Effects of cholesterol on laurdan fluorescence in sphingomyelin liposomes. A: Laurdan emission spectra in liposomes composed of pure sphingomyelin at 24°C (solid curve) and at 48°C (dashed curve). B: Laurdan generalized polarization (GP) assessed at multiple temperatures between 24°C and 48°C for the following final cholesterol mol%: 0% (filled square), 10% (filled triangle), 20% (open circle), 30% (open triangle), and 40% (filled diamond). C: Data analogous to those of panel B (5 mol% increments of cholesterol concentration) were used to generate a contour plot. The contour lines represent increments of 0.06 GP units. The assignment of phase regions [solid-ordered (S_o), liquid-disordered (l_d), and liquid-ordered (l_o)] is based on those identified previously in sphingomyelin/cholesterol vesicles (23).

disorder at higher temperature, as anticipated. The most abrupt change was recorded between 39°C and 42°C, which is expected around the melting temperature of sphingomyelin lipids (T_m 40.8°C) (22). The presence of cholesterol moderated this drop in GP (Fig. 1B).

The data in Fig. 1B can be viewed as a sphingomyelin/cholesterol phase map by representing them in a contour plot as shown in Fig. 1C. The phase regions identified previously (23) are labeled in the plot. Laurdan GP appeared to detect the transition from the liquid-ordered (l_o) to the liquid-disordered (l_d) phases in sphingomyelin vesicles but not the transition from the solid-ordered (S_o) to l_o. In other words, the contour lines all follow the same general trajectory, parallel to the order–disorder phase boundary, suggesting that laurdan is mostly sensitive to changes in the order of membrane lipids. This result is consistent with observations in liposomes composed of DPPC and cholesterol (12).

DPH anisotropy. Previously, nystatin was used in an analogous manner to detect changes in membrane fluidity independent of lipid order (13). Attempts at using nystatin in sphingomyelin vesicles were unsuccessful because of extremely low partitioning of the probe into the bilayer (i.e., fluorescence emission of the probe in the presence of liposomes was indistinguishable from background signal). DPH anisotropy was chosen as an alternative, because of its responsiveness to membrane fluidity, in addition to lipid order (19, 24).

Steady-state anisotropy values decreased with increasing temperature in pure sphingomyelin, with an abrupt drop between 39°C and 42°C (**Fig. 2A**). This observation, like the laurdan GP values, correlates with the melting temperature of sphingomyelin (22). As cholesterol concentration was increased to 40%, the decrease in anisotropy was attenuated and broadened over a wider range of temperatures.

The contour plot created based on DPH anisotropy values reveals that DPH detected changes both from the S_o to the l_o phases as well as from the l_o and S_o to the l_d (Fig. 2B). Hence, the contour lines do not all follow the same trajectory as they did in Fig. 1C.

MC540 emission spectra. **Figure 3A** shows MC540 emission spectra obtained with pure sphingomyelin liposomes at 24°C and 48°C. The distinctions between the temperatures consisted of a subtle reduction in emission intensity and a change in spectral shape. At 24°C, the maximum

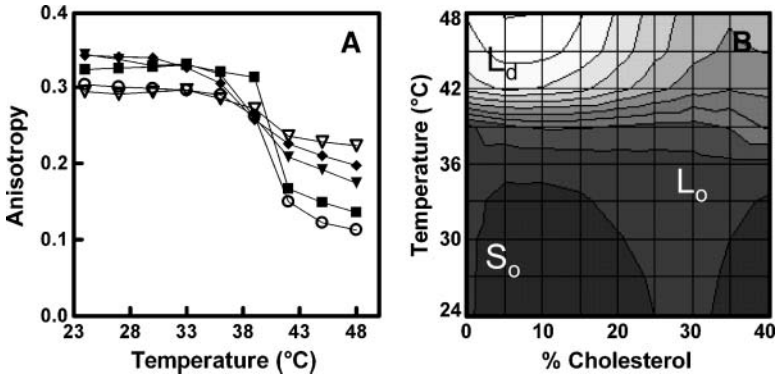

Fig. 2. Effects of cholesterol on diphenylhexatriene (DPH) anisotropy in sphingomyelin liposomes. A: Profile of DPH anisotropy in sphingomyelin liposomes containing 0% (filled square), 10% (filled triangle), 20% (open circle), 30% (open triangle), or 40% (filled diamond) cholesterol. B: DPH contour plot of data analogous to those of panel A (5 mol% increments of cholesterol). Contour lines represent increments of 0.018 anisotropy units.

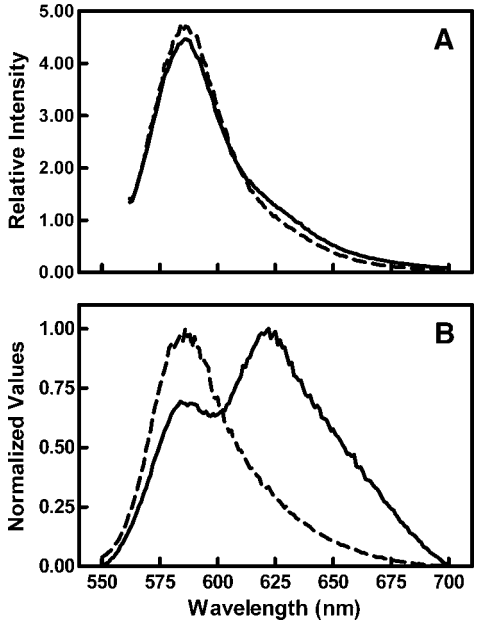

Fig. 3. Comparison of merocyanine 540 (MC540) spectral changes in sphingomyelin and in dipalmitoylphosphotidylcholine (DPPC) liposomes. A: MC540 emission spectra in liposomes composed of 100% sphingomyelin at 24°C (solid curve) and at 48°C (dashed curve). B: MC540 emission intensity in liposomes composed of 100% DPPC at 24°C (solid curve) and at 48°C (dashed curve) using data from (13). The data in this panel are normalized for comparison because of extensive intensity differences between the two spectra.

intensity was centered at 585 nm, with a small shoulder between 615 and 630 nm. At high temperature, the main peak remained, whereas the shoulder disappeared. In contrast to DPH and laurdan, which behaved similarly in sphingomyelin and DPPC liposomes (cf. Figs. 1, 2 with the data in Refs. 12, 13), MC540 spectra were markedly different between these two types of liposomes. Compared with data on DPPC vesicles (Fig. 3B) the amount of spectral shape change in sphingomyelin vesicles was much smaller.

Cholesterol concentration did not affect MC540 spectral shape or intensity in sphingomyelin vesicles. Spectral shape was quantified by calculating the ratio of intensity at 585 nm to that at 621 nm (**Fig. 4A**). As shown in the figure, the MC540 spectral ratio was mostly sensitive to temperature variation and minimally sensitive to cholesterol concentration. Consequently, lines in the contour plot are nearly parallel to the abscissa (Fig. 4B).

Sphingomyelin/cholesterol phase map. To create a composite of the effects of cholesterol and temperature on sphingomyelin liposomes and erythrocytes, color phase maps were generated. Laurdan fluorescence is represented in green. Increasing brightness corresponds to increased membrane disorder (diminished GP values). DPH anisotropy is shown in blue, with brightness indicating the level of fluidity and disorder sensed by the probe (increased brightness reflects lower anisotropy). Merocyanine fluorescence is given by the red hue, with brightness representing greater apparent spacing among lipids. The benefit of these maps is that they can combine parameters measured by different fluorescent probes into a collage that allows visual discernment of distinct phase regions. For example, overlaying the laurdan GP and DPH anisotropy data is helpful for distinguishing changes in order from fluidity. Previous work suggests that laurdan GP is most sensitive to lipid order (12, 13). Steady-state DPH anisotropy is sensitive to both, because it depends on the limiting anisotropy at infinite time (which is affected by order) as well as on the rotational correlation time (affected by membrane fluidity). As seen in **Fig. 5**, the color of the combined laurdan and DPH data remains at constant hue (aqua from overlay of green and blue), with varied intensity along the vertical edge of the figure where the S_o phase transitions to the l_d phase. However, along the horizontal edge of the diagram, in which the behavior transitions from l_d to l_o, the diagram hue changes from aqua to blue, representing a proportionally greater loss of green (laurdan) intensity as order decreases while fluidity remains high. Combining data from laurdan, DPH, and MC540 revealed four distinguishable regions of physical behavior for sphingomyelin/cholesterol liposomes (Fig. 5): S_o, l_d, and two types of l_o phase, one with apparent tight spacing among lipids [l_o(I)] and one inferring looser spacing [l_o(II)]. Because the cholesterol concentration increments were moderate (5 mol%), the data were smooth instead of punctuated as observed when tiny increments are used in the vicinity of concentration that generate cholesterol superlattices (25–27).

DPPC/DOPC/cholesterol phase map. The experiments shown in Figs. 1–5 were repeated with liposomes contain-

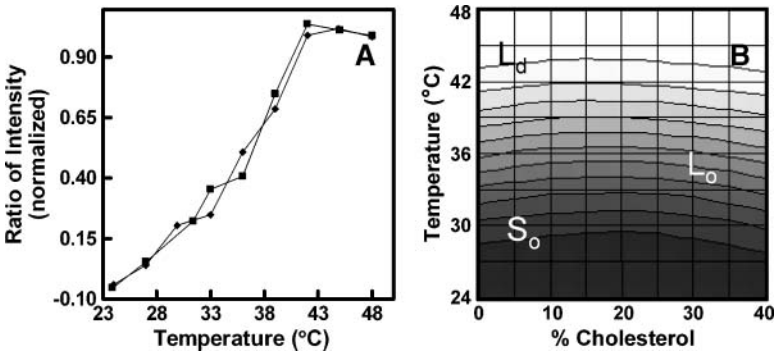

Fig. 4. Effects of cholesterol on MC540 fluorescence in sphingomyelin liposomes. A: MC540 ratio of intensity at 585 to 621 nm in sphingomyelin liposomes containing 0% (square) or 40% (diamond) cholesterol. The data were normalized to the maximum and minimum to account for small random variations between samples (complete range of ratios: 1.1 to 3.8). B: Contour plot generated from data analogous to those in Panel A (5 mol% cholesterol increments). Contour lines represent increments of 0.088 normalized ratio units.

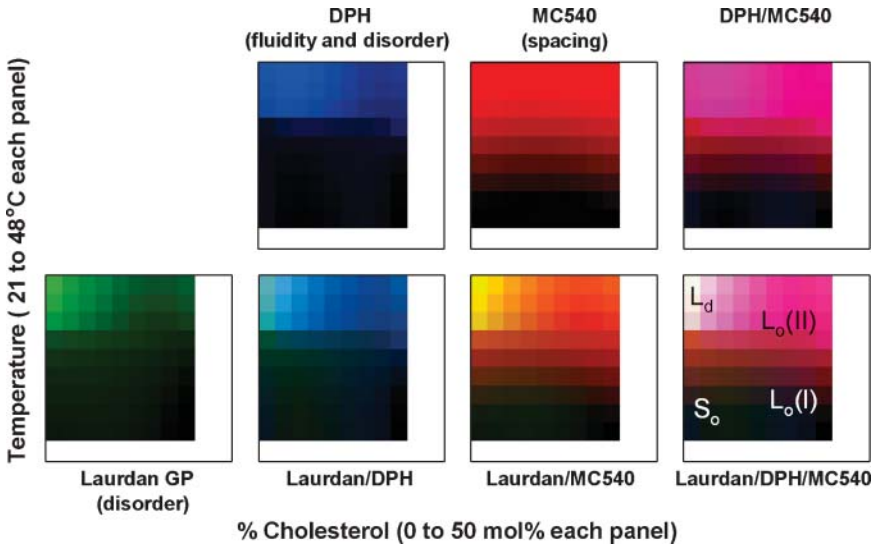

Fig. 5. Color phase maps of sphingomyelin liposomes. The data from the contour plots of Figs. 1, 2, and 4 were used to generate the maps. For each primary color, increasing brightness represents greater amounts of the physical parameter assessed by the corresponding probe (spanning the range indicated from lowest to greatest brightness): laurdan, disorder (green, 0.76 to 0.039 GP units); DPH, fluidity and disorder (blue, 0.34 to 0.12 anisotropy units), MC540, spacing (red, −0.025 to 1.036 normalized ratio units, as in Fig 4).

ing equimolar mixtures of DPPC and DOPC with various concentrations of cholesterol. As reported previously, this combination of saturated (DPPC) and monounsaturated (DOPC) phospholipids allows one to explore the behavior of the fluorescent probes under conditions of phase coexistence (28) At low cholesterol concentrations (below 10 mol%), the system consists of S_o and l_d phases. Between 10 mol% and 45 mol% cholesterol, there is coexistence of l_d and l_o phases. At higher cholesterol contents, the liposomes would display solely l_o properties. The results of these experiments are summarized as color phase maps, shown in **Fig. 6**. Compared with Fig. 5, there was much less diversity of fluorescence behavior across the cholesterol and temperature ranges tested. Most of the variations in fluorescence properties were attributed to the values of laurdan GP. DPH anisotropy values followed trends similar to those of laurdan GP, but with a smaller range of variation. Merocyanine fluorescence was essentially con-

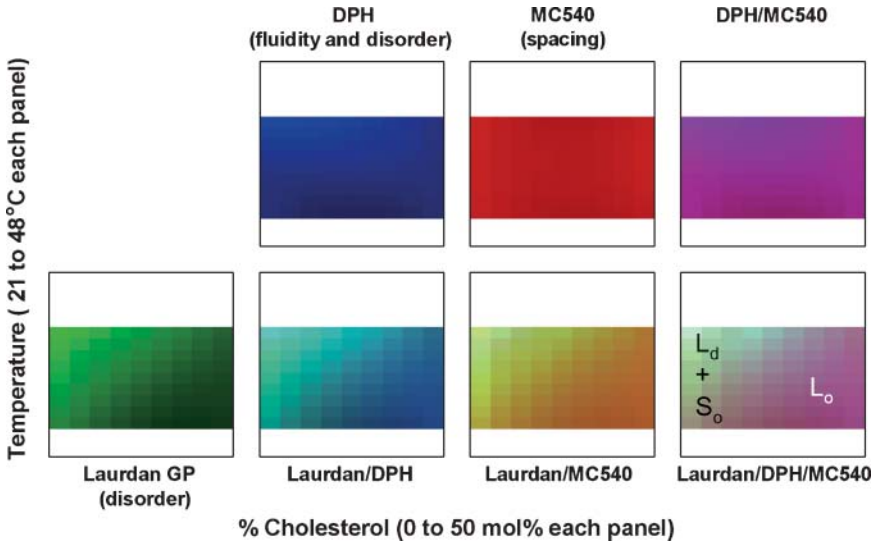

Fig. 6. Color phase maps of DPPC/dioleoylphosphatidylcholine (DOPC) liposomes. Data were gathered for each of the fluorescent probes and contour plots generated as explained in the legends to Figs. 1, 2, 4 for liposomes containing equimolar DPPC and DOPC and either 0, 30 or 50 mol% cholesterol for multiple temperatures between 25°C and 40°C. Phase maps were then created as explained in the legend to Fig. 5 using the same brightness scales.

stant throughout the range of experimental conditions. In particular, the temperature sensitivity displayed in Fig. 5 did not occur with DPPC/DOPC liposomes.

Erythrocytes depleted of cholesterol

A broad range of experimental conditions have been employed in the past using MBCD to deplete cell membranes of cholesterol (29). For example, MBCD concentrations up to 20 mM have been used, and incubation times have varied from 30 min to 8 h (29). Because MBCD functions as a sink for cholesterol, the extraction efficiency probably depends more on the ratio of the amount of cell membrane to the amount of MBCD than on the absolute MBCD concentration. Accordingly, we elected to characterize a protocol for our own system rather than try to select from the various published procedures. As shown in **Fig. 7**, the amount of cholesterol removed from human erythrocytes varied linearly with MBCD concentration under the conditions used for this study (0–1 mM MBCD, 0.15 hct, 30 min, 37°C). At the highest concentration of MBCD used (1 mM), about 70% of membrane cholesterol was removed from the cells.

Figure 8 displays profiles of laurdan GP (Panel A), DPH anisotropy (Panel B), and MC540 intensity (Panel C) as a function of temperature in erythrocytes at various membrane cholesterol contents. The corresponding contour plots are shown in Fig. 8D–F. Note that the contour plots are constructed to span the range of values observed in erythrocytes rather than being adjusted to the same scales used for the sphingomyelin liposomes (Figs. 1–4). In fact, the scales for the liposomes cover a range about 3.5-fold greater than those for the erythrocytes, as noted previously (13). Thus, the variations observed with the erythrocytes are about one-fourth the magnitude of those observed with liposomes over the same temperature range.

All three probes displayed behavior toward temperature similar to that reported previously (13). Laurdan GP decreased as temperature was raised, DPH anisotropy also decreased, and MC540 intensity increased. Removal of cholesterol had a relatively substantial effect in reducing laurdan GP values (Fig. 8A, D). The anisotropy of DPH, however, was much less sensitive to membrane cholesterol content (Fig. 8B, E). The primary response was a lowering of the temperature range of greatest anisotropy change (Fig. 8B). As seen in Fig. 8F, cholesterol depletion caused apparent biphasic effects on the response of MC540 to temperature changes. At the extremes of cholesterol concentration, the profile of MC540 intensity as a function of temperature was nearly identical. However, at intermediate cholesterol concentrations (~30%), the profile was shifted to lower temperatures.

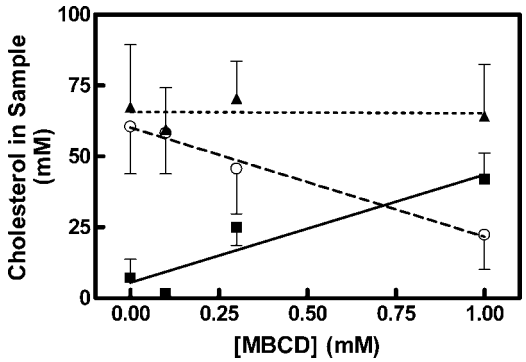

Fig. 7. Relationship between methyl-β-cyclodextrin (MBCD) concentration and the amount of cholesterol extracted from human erythrocytes. Erythrocytes were extracted with the indicated concentrations of MBCD and assayed for residual cholesterol content in the cell membrane (circle) and that in the extract (square) as described in Materials and Methods. The triangles demonstrate total cholesterol (residual + extracted) in each sample (mean ± SE, n = 4). The lines are linear regressions.

Previous microscopy studies with laurdan have demonstrated that the distribution of GP values is not uniform across the surface of the erythrocyte (12, 30–32). In general, high GP values are found along the perimeter of the erythrocyte disk. **Figure 9A** displays an example of this observation. The somewhat higher GP values located at the upper left and lower right edges of the cells in the image are due to the fact that the laser source exciting the samples is polarized. Although efforts are made to depolarize the light with optical filters, the depolarization is only partial, resulting in preferential excitation of more-disordered fluorophores along the perpendicular axis. Assuming that high GP represents regions of more-ordered lipids, and given the well-established effect of cholesterol in increasing membrane order (33), it was reasonable to address the question of whether cholesterol removal alters membrane properties only in regions of high laurdan GP or whether it does so more uniformly. Figure 9B is a sample image of erythrocytes treated with 1 mM MBCD to remove about 70% of membrane cholesterol. The apparent reduction in membrane order suggested by the data in Fig. 8A and D is visible in the image as a change in GP values across the cell membrane. Figure 9C–E display histograms of cell GP distribution with and without MBCD treatment. The different panels compare GP values for the total surface of the cells, the central region, and the perimeter using data pooled from multiple images such as those shown in Fig. 9A.

The results for erythrocytes are summarized in color phase maps (**Figs. 10, 11**). Figure 10 presents the results in the expanded scale of Fig. 8 to emphasize differences. Figure 11 shows the same data on the scale of Fig. 5 for more direct comparison to the liposomes.

An important issue with fluorescence measurements with erythrocytes is discerning whether the results observed represent the behavior of the outer membrane leaflet, the inner leaflet, or an average of the two. Because MC540 would have limited ability to cross the membrane and enter intact cells (verified for other cell types by confocal microscopy, not shown), its fluorescence reports only the outer leaflet. In contrast, the more hydrophobic laurdan and DPH do cross the cell membrane and presumably report behavior from both leaflets. In an effort to provide some additional basis for interpretation of the data in Figs. 10 and 11, we created liposomes containing

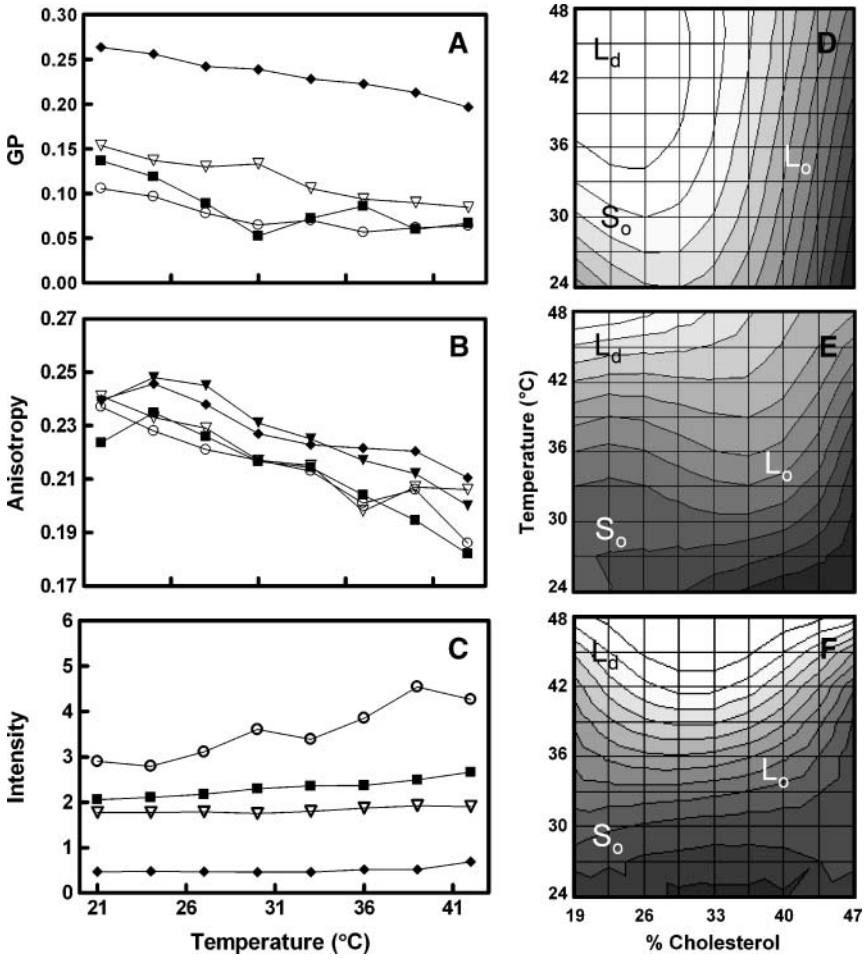

Fig. 8. Effects of cholesterol depletion on the temperature dependence of laurdan GP values (A), DPH anisotropy (B), and MC540 emission intensity (C) in human erythrocytes. Cell cholesterol was extracted with 0 (diamond), 0.1 mM (filled triangle), 0.3 mM (open triangle), 0.6 mM (circle) or 1.0 mM (square) MBCD from erythrocytes. D–F: Contour plots were generated from the data of Panels A–C. D: Laurdan GP values with contour lines representing 0.020 increments in GP. E: DPH anisotropy with contour lines representing 0.005 increments in anisotropy. F: MC540 intensities with contour lines representing increments of 0.010 normalized integral values. The cholesterol content values were calculated using the data of Fig. 7, assuming an initial cholesterol concentration of 46.8% (54, 55). Data at each MBCD concentration were averaged from six or more independent blood samples.

lipids representative of the outer or inner leaflets of the erythrocyte membrane (34, 35) and repeated the measurements with DPH and laurdan at both high and low cholesterol concentrations. As shown in **Fig. 12**, the liposomes simulating the outer leaflet behaved similar to the DPPC/DOPC liposomes in Fig. 6 (larger change in laurdan GP than DPH anisotropy). This observation is logical, because the composition of the outer leaflet contains mixtures of saturated and unsaturated phospholipids analogous to those in the DPPC/DOPC vesicles. The results for the inner leaflet liposomes were qualitatively similar to those for the outer leaflet with respect to laurdan, although the overall GP values were lower (more disordered). DPH anisotropy responded more to cholesterol reduction for the inner leaflet liposomes than for the outer. Consequently, the hue for overlayed data switched from green-dominated for the outer leaflet as cholesterol concentration was increased, whereas it remained blue-dominated at both low and high cholesterol for the liposomes simulating the inner leaflet.

DISCUSSION

Liposomes

The effect of cholesterol on membrane physical properties has been studied for many years. The presence of cholesterol in membranes broadens the solid-to-liquid phase transition through interactions between the sterol and the phospholipids (8, 22). Theoretical analyses of the actions of cholesterol have revealed a variety of both general and specific effects, depending on the membrane composition (e.g., see Refs. 25, 36, 37). At concentrations above 20 mol% to 25 mol%, it induces formation of an

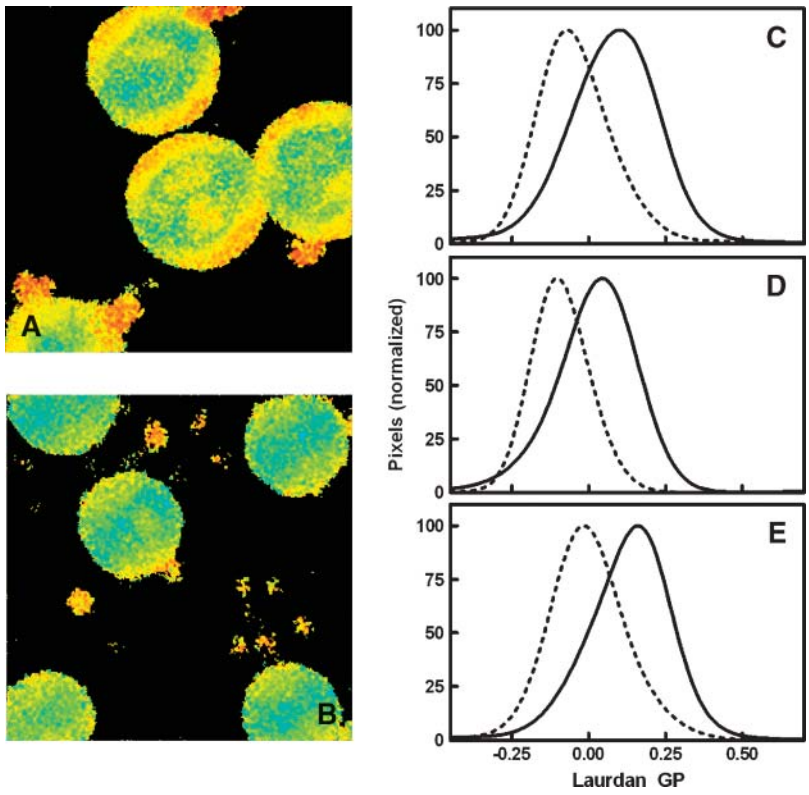

Fig. 9. Two-photon false color images of laurdan GP in human erythrocytes treated without (A) or with 1.0 mM MBCD (B). Images were acquired at 37°C, with pure red representing maximum GP (1.0) and pure blue representing minimum GP (−1.0). C–E: Histograms of normalized pixel GP were generated and averaged for whole cells (C), the middle region of cells (D), and perimeter region (E) from several images (total of 21 control cells and 15 MBCD-treated cells). Solid lines represent control cells, and dotted lines represent cells treated with MBCD.

l_o phase (38). Whether this l_o phase represents a separate thermodynamic phase with boundaries and a mixed-phase region distinguishing it from the l_d phase is a matter of ongoing discussion and probably depends on the details of the experimental model (36, 37, 39). An interesting prediction of theoretical calculations is that cholesterol molecules induce formation of superlattice structures at specific concentrations defined by geometric models (25, 26, 40). The actual presence of such structures in artificial bilayers has been established by a variety of experimental methods (25, 41, 42). Furthermore, it has been shown recently that the ability to detect the superlattices by fluorescence spectroscopy involves a number of issues in addition to cholesterol concentration, including thermal history, time since liposome formation, and whether lipid oxidation has been successfully prevented. In the current study, we elected to focus our attention on the overall trends in membrane properties across major phase regions rather than attempt to isolate the behavior at critical cholesterol concentrations corresponding to superlattices. Lipid oxidation was avoided by using liposomes the same day they were prepared from fresh cholesterol (43).

The combined phase map shown in Fig. 5 is simpler than that obtained with DPPC/cholesterol liposomes, where eight identifiable regions were observed, the four found here with sphingomyelin plus four others (13). One of the DPPC regions absent in Fig. 5 represents the P_β' or ripple phase. This result corroborates a previous calorimetric observation that sphingomyelin liposomes do not exhibit a pretransition from S_o to P_β' phases (22). The other three differences between the composite phase maps of sphingomyelin liposomes and DPPC vesicles correspond to presumed mixed-phase regions between S_o or l_d and the l_o phases in the DPPC system. Nevertheless, these mixed-phase regions were not well-defined, perhaps supportive of a continuous (single-phase) model of changes in lipid behavior upon addition of cholesterol rather than a model corresponding to coexistence of discrete phases, especially with respect to the l_d–l_o transition (13, 36, 37). The current observations with sphingomyelin liposomes are even more suggestive of a continuous model (Fig. 5).

We were surprised to discover that several fluorescent probes that bind well to DPPC liposomes did not interact similarly with sphingomyelin. For example, prodan and nystatin fluorescence was indistinguishable from background and completely unusable. Even though MC540 fluorescence was sufficient in sphingomyelin liposomes to make judgments concerning lipid spacing, the spectral responses to the main phase transition were much smaller

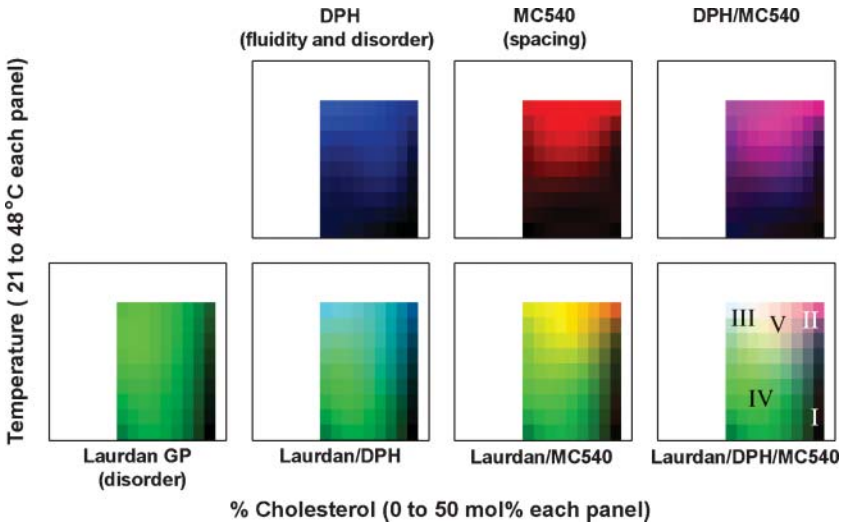

Fig. 10. Color phase maps of human erythrocytes. The maps were generated as in Fig. 5 using the data of Fig. 8. The brightness scale is set at the maxima and minima of the erythrocyte data: 0.26 to 0.022 GP units for laurdan, 0.24 to 0.18 anisotropy units for DPH, and 0.64 to 0.89 normalized units for MC540 (see Fig. 4 for details).

than with DPPC liposomes (Fig. 3). The common property of these three probes is that they all interact, at least under certain conditions, with the surface of the bilayer. Inferences from previous molecular simulations of sphingomyelin model membranes may explain these observations. Those simulations revealed additional intramolecular and intermolecular hydrogen bonding established by the nitrogen group of sphingomyelin that would not be possible for phosphatidylcholine (44, 45). These hydrogen bonds among sphingomyelin molecules are likely to restrict partitioning of prodan and nystatin while limiting MC540 to adsorption superficial to the bonds. These constraints would prevent MC540 from partitioning at an orientation perpendicular to the membrane surface. This argument explains the subtlety of spectral shape changes in Fig. 3A, because the spectral peak at about 620 nm is reported to depend on the perpendicular orientation (16).

An observation that appears relevant to both DPPC and sphingomyelin liposomes is the two variations of the l_o phase identified by the MC540 data in Fig. 5, l_o(I) and l_o(II). Control experiments reported in the previous DPPC study demonstrated that these results are not an artifact of direct effects of temperature on the probe's fluorescence (13). Instead, we interpreted the data to suggest that the spacing between lipid molecules increases at the melting temperature of the pure phospholipid regardless of the presence of cholesterol (13). This interpretation corroborates results in which intermolecular

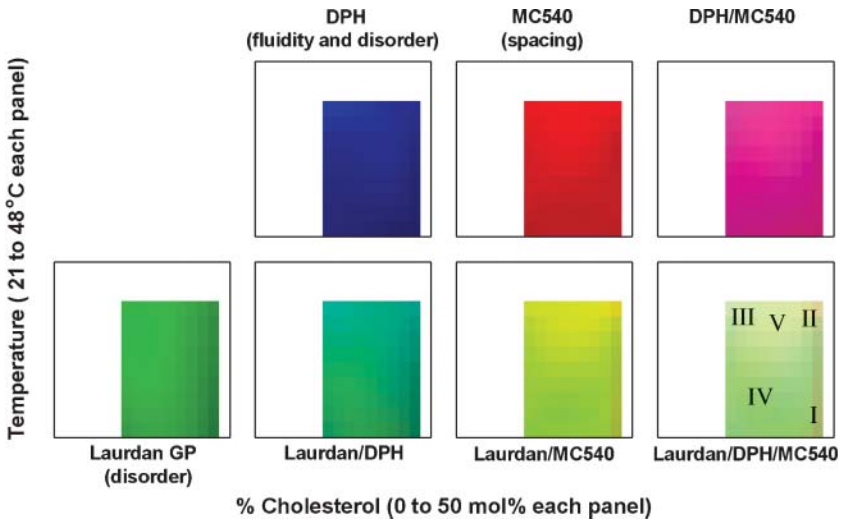

Fig. 11. Erythrocyte phase maps shown on same scale as liposomes. The data of Fig. 10 were adjusted to the same brightness scale used in Fig. 5.

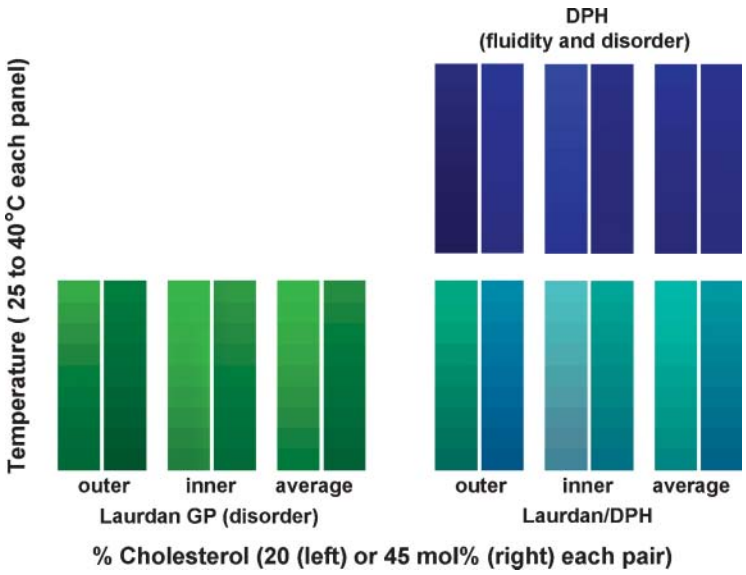

Fig. 12. Color profiles of liposomes simulating the inner and outer leaflets of erythrocyte membranes at low and high cholesterol. Data were gathered as explained in the legends to Figs. 1 and 2 using laurdan or DPH. outer: 1: 0.93 DOPC and palmitoyl sphingomyelin with 20 mol% or 45 mol% cholesterol. inner: 1:2.1:3.8 DOPC, porcine brain phosphatidylserine, and bovine liver phosphatidylethanolamine with 20 mol% or 45 mol% cholesterol. Data were obtained at multiple temperatures between 25°C and 45°C. Color profiles were then created as explained in the legend to Fig. 5, using the same brightness scale. Because only two cholesterol concentrations were used, data were smoothed by nonlinear regression in only one dimension (temperature).

distances were measured by X-ray diffraction (46). Interestingly, the transition between these two apparent phase regions seemed more subtle with sphingomyelin liposomes (Fig. 5) than with DPPC liposomes (13).

The results with DPPC/DOPC liposomes (Fig. 6) were less complex than those with the sphingomyelin vesicles and consistent with previous studies using such mixtures (28). This observation makes sense, because the ternary mixtures used would not be expected to generate either a pure S_o phase or a pure l_d phase under the conditions studied. The dominance of laurdan in terms of changes recorded across temperature and cholesterol concentration presumably reflects the sensitivity of this probe to lipid order (12). Thus, the membrane became more disordered as temperature increased at low cholesterol, reflecting disordering of the DPPC lipids in the coexistence region (l_d + S_o). Likewise, it became more ordered as cholesterol concentration was raised, because of increasing prevalence of l_o properties, as expected (28). Membrane fluidity would be expected to remain more constant through the phase map, because all phase regions represented are at least partially liquid. Interestingly, the temperature sensitivity displayed for MC540 in Fig. 5 did not occur with DPPC/DOPC vesicles, suggesting that the presence of the unsaturated lipid may preclude changes in lipid spacing observed with pure saturated phospholipids.

Erythrocytes

To our knowledge, this is the first time that a phase map has been generated for intact erythrocytes. The composite plot shows five identifiable regions of lipid behavior. Untreated erythrocytes display two regions (I and II in Figs. 10 and 11), as described previously (13). Region I is characterized by relatively low spacing, low fluidity, and high order. Region II is described by greater fluidity and spacing, with a comparatively smaller reduction in order. Region III is observed at high temperature and when significant amounts of cholesterol are depleted from the membrane. Relative to Region II, it displays lower order and higher fluidity, with the same level of apparent lipid spacing. Region IV, which seems to dominate the phase map, describes membrane behavior with diminished order compared with Regions I and II but also with lower fluidity and tighter spacing than Regions I and III. A fifth region is identified at moderate cholesterol concentrations (~30%). It appears to have the same properties as Region III, but with greater spacing among phospholipids. Other color variations in the composite phase map presumably reflect smooth transitions among these regions.

The regions displayed in Figs. 10 and 11 bear some qualitative similarities to the phase maps of sphingomyelin (Fig. 5) and DPPC/DOPC liposomes (Fig. 6). For example, Regions I and II compare well with the two types of l_o phase observed in the sphingomyelin liposomes. Likewise, Region III in the erythrocytes displays relative behavior reminiscent of the l_d phase. In fact, it is likely that all three regions with decreased cholesterol reflect lipid properties influenced heavily by disordered unsaturated lipids (III, IV, and V). Comparison to the DPPC/DOPC vesicles (Fig. 6) supports this idea, especially in terms of the smooth transition from green-dominated to blue-dominated hues in the combined laurdan and DPH data. Nevertheless, the absolute level of membrane order displayed by the erythrocytes was less than the average level observed for the liposomes, regardless of the presence of unsaturated phospholipids (Fig. 11). Furthermore, it is certain that the observed properties, regardless of cholesterol concentration, are impacted by the heterogeneity of membrane lipids, the presence of integral membrane proteins, the transbilayer asymmetry of phospholipid species, and interactions with the cytoskeleton.

The data in Fig. 12 attempt to address, at least in part, the issue of transbilayer asymmetry. The results suggest that the differences between the two leaflets with respect to the lipids are likely to be small, although the observa-

tions for the outer membrane resemble the data of Figs. 10 and 11 more than do those for the inner membrane. Moreover, evidence and analysis from studies comparing the leaflets of intact bilayers suggest that the two may be coupled, thus reducing transbilayer differences in properties (47, 48).

There are at least two additional observations apparent in Figs. 10 and 11 that are not adequately rationalized by an appeal to simple liposome systems and probably reflect the other complexities inherent in biological membranes. One such observation is revealed by comparing the data with laurdan and DPH at low temperature and cholesterol concentration in region IV. The color hue of the combined DPH and laurdan data in Fig. 10 transitions from aqua in Regions I, II, III, and V to green in Region IV. These results may be interpreted to suggest that the fluidity of the membrane has decreased, whereas order has remained relatively constant. Such a change is observed in artificial membranes during the transition from the l_o to the S_o phase upon reduction in cholesterol concentration at low temperature. However, in the erythrocytes, the membrane appears much more disordered than for an S_o phase, and a simple explanation for why removal of cholesterol or lowering of temperature would make the membrane less fluid while remaining disordered is difficult to conceive. Perhaps it reflects changes in average responses as different populations (microdomains) of lipids respond to cholesterol removal and/or temperature reduction. It may also represent temperature-dependent changes in cytoskeletal interactions. It must be remembered that these interpretations assume that DPH and laurdan both partition into the same microenvironments in the membrane. Although this assumption is reasonable, given the behavior of the two probes in artificial systems, it cannot easily be proven for biological membranes.

The second unreconciled observation is the dependence of MC540 fluorescence on cholesterol concentration in the erythrocytes. The temperature at which lipid spacing appeared to increase was lowered as cholesterol was removed from the cells. Moreover, this trend reversed near the lowest cholesterol concentration (Fig. 10). A possible explanation is that cholesterol may have a condensing effect on certain lipid populations in the membrane at high concentration and an expanding effect on other populations at lower concentration.

One reason for the apparent better match between the outer membrane from Fig. 12 and the erythrocyte data (Figs. 10, 11) could be the fact that intracellular hemoglobin may quench the fluorescence of DPH and laurdan in the inner leaflet through energy transfer (49). Moreover, optical absorbance of emitted light by hemoglobin also alters the measured value of laurdan GP (20). Means to correct for these phenomena have been published (20, 50). However, we elected not to employ these corrections for the following reasons. First, all experiments were conducted at the same hct so that the hemoglobin concentration would not be a variable. Corrections would therefore affect the average level of anisotropy and laurdan GP but not the changes observed under the various conditions. Second, the effect of hemoglobin on DPH anisotropy is much smaller than the variation between blood samples (50); applying a correction thus has as much chance of making the data worse as it does improving it. Third, although the effects of hemoglobin on laurdan GP are greater than on DPH, the proposed correction requires too many assumptions of uncertain validity to merit its use when hemoglobin concentrations are constant (20). An alternative would be to use erythrocyte ghosts instead of intact cells. Although the challenges associated with hemoglobin would be eliminated by that decision, prior experience indicates that effects of ghost preparation on membrane properties can be very large. Among the properties altered are laurdan GP, anisotropy, and transbilayer distribution of phosphatidylserine (20). Thus, it must be recognized that the changes in laurdan GP and DPH anisotropy reported here are more meaningful than the absolute average level of these two measurements, especially for laurdan. In general, the laurdan GP values should probably be about 0.1 units higher than shown in Figs. 10 and 11 (20). A difference of that magnitude would bring the results for erythrocytes closer to those obtained from fluid artificial membranes (Figs. 6, 12), but the cell membranes would still display greater disorder on average than did the liposomes.

An important issue with respect to MBCD is whether it extracts cholesterol uniformly from the membrane or selectively from specific compartments or domains (29). This consideration is particularly important in studies of nucleated cells that possess multiple membranes. Nevertheless, recent evidence from erythrocytes suggests that extraction originates from a single uniform pool (51). The laurdan two-photon data presented here (Fig. 9) show that the central and perimeter regions responded similarly to cholesterol extraction by MBCD, supporting this latter interpretation. These data also suggest that the well-documented observation that erythrocyte membranes are more-ordered along the perimeter of the disc (Fig. 9) (12, 30–32) is not explained by substantially greater cholesterol content in this region of the membrane.

A caveat for this and other studies using cyclodextrins is their ability to extract other lipids, depending on the concentration and incubation time (as reviewed in Ref. 29). This concern becomes greater when high concentrations and long incubation times are employed. However, the conditions selected for this study are likely to remove only a few percent of membrane phospholipids, based on previous measurements (52, 53) and the efficiency of cholesterol extraction observed in Fig. 7. Nevertheless, we cannot exclude the possibility that additional lipids extracted in our experiments contribute to the results shown for erythrocytes. This consideration must always temper conclusions from experiments with MBCD.

In summary, these data reveal significant effects of cholesterol on the physical behavior of membrane lipids in erythrocytes, providing further evidence that the ordering effect of the sterol applies to biological membranes. In fact, the results demonstrate similarities between the behavior of erythrocyte and artificial membranes, not-

withstanding the obvious compositional differences between the two. Nevertheless, the interesting novel observations in the cells remind us that the complexity of biological membranes accommodates effects of cholesterol not observed in liposomes. These data provide a framework for studies relating membrane physical properties to cellular and biochemical functions that depend on the presence of cholesterol.

Two-photon experiments were performed at the Laboratory for Fluorescence Dynamics (LFD) at the University of California, Irvine. The authors gratefully acknowledge the assistance of LFD personnel, especially Enrico Gratton (Principal Investigator), Susana Sanchez (User Coordinator), Oliver Holub, and Theodore Hazlett (Director). The authors also acknowledge the technical assistance of Andrew Noble from the Department of Biology at Utah Valley State College.

REFERENCES

1. Koval, M., and R. E. Pagano. 1991. Intracellular transport and metabolism of sphingomyelin. *Biochim. Biophys. Acta.* **1082:** 113–125.
2. Simons, K., and E. Ikonen. 1997. Functional rafts in cell membranes. *Nature.* **387:** 569–572.
3. Schroeder, R. J., S. N. Ahmed, Y. Zhu, E. London, and D. A. Brown. 1998. Cholesterol and sphingolipid enhance the Triton X-100 insolubility of glycosylphosphatidylinositol-anchored proteins by promoting the formation of detergent-insoluble ordered membrane domains. *J. Biol. Chem.* **273:** 1150–1157.
4. Brown, D. A., and E. London. 1998. Structure and origin of ordered lipid domains in biological membranes. *J. Membr. Biol.* **164:** 103–114.
5. Xu, X., and E. London. 2000. The effect of sterol structure on membrane lipid domains reveals how cholesterol can induce lipid domain formation. *Biochemistry.* **39:** 843–849.
6. Guo, W., V. Kurze, T. Huber, N. H. Afdhal, K. Beyer, and J. A. Hamilton. 2002. A solid-state NMR study of phospholipid-cholesterol interactions: sphingomyelin-cholesterol binary systems. *Biophys. J.* **83:** 1465–1478.
7. Holopainen, J. M., A. J. Metso, J. P. Mattila, A. Jutila, and P. K. Kinnunen. 2004. Evidence for the lack of a specific interaction between cholesterol and sphingomyelin. *Biophys. J.* **86:** 1510–1520.
8. Aittoniemi, J., P. S. Niemela, M. T. Hyvonen, M. Karttunen, and I. Vattulainen. 2007. Insight into the putative specific interactions between cholesterol, sphingomyelin, and palmitoyl-oleoyl phosphatidylcholine. *Biophys. J.* **92:** 1125–1137.
9. Dietrich, C., L. A. Bagatolli, Z. N. Volovyk, N. L. Thompson, M. Levi, K. Jacobson, and E. Gratton. 2001. Lipid rafts reconstituted in model membranes. *Biophys. J.* **80:** 1417–1428.
10. Filippov, A., G. Oradd, and G. Lindblom. 2003. The effect of cholesterol on the lateral diffusion of phospholipids in oriented bilayers. *Biophys. J.* **84:** 3079–3086.
11. Calhoun, W. I., and G. G. Shipley. 1979. Sphingomyelin–lecithin bilayers and their interaction with cholesterol. *Biochemistry.* **18:** 1717–1722.
12. Harris, F. M., K. B. Best, and J. D. Bell. 2002. Use of laurdan fluorescence intensity and polarization to distinguish between changes in membrane fluidity and phospholipid order. *Biochim. Biophys. Acta.* **1565:** 123–128.
13. Wilson-Ashworth, H. A., Q. Bahm, J. Erickson, A. Shinkle, M. P. Vu, D. Woodbury, and J. D. Bell. 2006. Differential detection of phospholipid fluidity, order, and spacing by fluorescence spectroscopy of bis-pyrene, prodan, nystatin, and merocyanine 540. *Biophys. J.* **91:** 4091–4101.
14. Parasassi, T., G. De Stasio, G. Ravagnan, R. M. Rusch, and E. Gratton. 1991. Quantitation of lipid phases in phospholipid vesicles by the generalized polarization of laurdan fluorescence. *Biophys. J.* **60:** 179–189.
15. Stillwell, W., S. R. Wassall, A. C. Dumaual, W. D. Ehringer, C. W. Browning, and L. J. Jenski. 1993. Use of merocyanine (MC540) in quantifying lipid domains and packing in phospholipid vesicles and tumor cells. *Biochim. Biophys. Acta.* **1146:** 136–144.
16. Yu, H., and S. W. Hui. 1992. Merocyanine 540 as a probe to monitor the molecular packing of phosphatidylcholine: a monolayer epifluorescence microscopy and spectroscopy study. *Biochim. Biophys. Acta.* **1107:** 245–254.
17. Jensen, L. B., N. K. Burgess, D. D. Gonda, E. Spencer, H. A. Wilson-Ashworth, E. Driscoll, M. P. Vu, J. L. Fairbourn, A. M. Judd, and J. D. Bell. 2005. Mechanisms governing the level of susceptibility of erythrocyte membranes to secretory phospholipase A2. *Biophys. J.* **88:** 2692–2705.
18. Bligh, E. G., and W. J. Dyer. 1959. A rapid method of total lipid extraction and purification. *Can. J. Biochem. Physiol.* **37:** 911–917.
19. Dale, R. E., L. A. Chen, and L. Brand. 1977. Rotational relaxation of the "microviscosity" probe diphenylhexatriene in paraffin oil and egg lecithin vesicles. *J. Biol. Chem.* **252:** 7500–7510.
20. Harris, F. M., S. K. Smith, and J. D. Bell. 2001. Physical properties of erythrocyte ghosts that determine susceptibility to secretory phospholipase A2. *J. Biol. Chem.* **276:** 22722–22731.
21. Yu, W., P. T. So, T. French, and E. Gratton. 1996. Fluorescence generalized polarization of cell membranes: a two-photon scanning microscopy approach. *Biophys. J.* **70:** 626–636.
22. Nyholm, T. K., M. Nylund, and J. P. Slotte. 2003. A calorimetric study of binary mixtures of dihydrosphingomyelin and sterols, sphingomyelin, or phosphatidylcholine. *Biophys. J.* **84:** 3138–3146.
23. de Almeida, R. F., A. Fedorov, and M. Prieto. 2003. Sphingomyelin/phosphatidylcholine/cholesterol phase diagram: boundaries and composition of lipid rafts. *Biophys. J.* **85:** 2406–2416.
24. Veatch, W. R., and L. Stryer. 1977. Effect of cholesterol on the rotational mobility of diphenylhexatriene in liposomes: a nanosecond fluorescence anisotrophy study. *J. Mol. Biol.* **117:** 1109–1113.
25. Virtanen, J. A., M. Ruonala, M. Vauhkonen, and P. Somerharju. 1995. Lateral organization of liquid-crystalline cholesterol-dimyristoylphosphatidylcholine bilayers. Evidence for domains with hexagonal and centered rectangular cholesterol superlattices. *Biochemistry.* **34:** 11568–11581.
26. Liu, F., I. P. Sugar, and P. L. Chong. 1997. Cholesterol and ergosterol superlattices in three-component liquid crystalline lipid bilayers as revealed by dehydroergosterol fluorescence. *Biophys. J.* **72:** 2243–2254.
27. Wang, M. M., M. Olsher, I. P. Sugar, and P. L. Chong. 2004. Cholesterol superlattice modulates the activity of cholesterol oxidase in lipid membranes. *Biochemistry.* **43:** 2159–2166.
28. Veatch, S. L., and S. L. Keller. 2003. Separation of liquid phases in giant vesicles of ternary mixtures of phospholipids and cholesterol. *Biophys. J.* **85:** 3074–3083.
29. Zidovetzki, R., and I. Levitan. 2007. Use of cyclodextrins to manipulate plasma membrane cholesterol content: evidence, misconceptions and control strategies. *Biochim. Biophys. Acta.* **1768:** 1311–1324.
30. Parasassi, T., E. Gratton, W. M. Yu, P. Wilson, and M. Levi. 1997. Two-photon fluorescence microscopy of laurdan generalized polarization domains in model and natural membranes. *Biophys. J.* **72:** 2413–2429.
31. Smith, S. K., A. R. Farnbach, F. M. Harris, A. C. Hawes, L. R. Jackson, A. M. Judd, R. S. Vest, S. Sanchez, and J. D. Bell. 2001. Mechanisms by which intracellular calcium induces susceptibility to secretory phospholipase A2 in human erythrocytes. *J. Biol. Chem.* **276:** 22732–22741.
32. Vest, R. S., L. J. Gonzales, S. A. Permann, E. Spencer, L. D. Hansen, A. M. Judd, and J. D. Bell. 2004. Divalent cations increase lipid order in erythrocytes and susceptibility to secretory phospholipase A2. *Biophys. J.* **86:** 2251–2260.
33. Miao, L., M. Nielsen, J. Thewalt, J. H. Ipsen, M. Bloom, M. J. Zuckermann, and O. G. Mouritsen. 2002. From lanosterol to cholesterol: structural evolution and differential effects on lipid bilayers. *Biophys. J.* **82:** 1429–1444.
34. Ingraham, L. M., C. P. Burns, L. A. Boxer, R. L. Baehner, and R. A. Haak. 1981. Fluidity properties and liquid composition of erythrocyte membranes in Chediak-Higashi syndrome. *J. Cell Biol.* **89:** 510–516.
35. Owen, J. S., K. R. Bruckdorfer, R. C. Day, and N. McIntyre. 1982. Decreased erythrocyte membrane fluidity and altered lipid composition in human liver disease. *J. Lipid Res.* **23:** 124–132.
36. McConnell, H., and A. Radhakrishnan. 2006. Theory of the deuterium NMR of sterol-phospholipid membranes. *Proc. Natl. Acad. Sci. USA.* **103:** 1184–1189.

37. Veatch, S. L., and S. L. Keller. 2005. Seeing spots: complex phase behavior in simple membranes. *Biochim. Biophys. Acta.* **1746:** 172–185.
38. Crane, J. M., and L. K. Tamm. 2004. Role of cholesterol in the formation and nature of lipid rafts in planar and spherical model membranes. *Biophys. J.* **86:** 2965–2979.
39. Elliott, R., I. Szleifer, and M. Schick. 2006. Phase diagram of a ternary mixture of cholesterol and saturated and unsaturated lipids calculated from a microscopic model. *Phys. Rev. Lett.* **96:** 098101.
40. Huang, J. 2002. Exploration of molecular interactions in cholesterol superlattices: effect of multibody interactions. *Biophys. J.* **83:** 1014–1025.
41. Cannon, B., A. Lewis, J. Metze, V. Thiagarajan, M. W. Vaughn, P. Somerharju, J. Virtanen, J. Huang, and K. H. Cheng. 2006. Cholesterol supports headgroup superlattice domain formation in fluid phospholipid/cholesterol bilayers. *J. Phys. Chem. B.* **110:** 6339–6350.
42. Sengupta, P., R. R. Singh, D. L. Cox, and A. Slepoy. 2004. Lateral organization of cholesterol molecules in lipid-cholesterol assemblies. *Phys. Rev. E Stat. Nonlin. Soft Matter Phys.* **70:** 021902.
43. Venegas, B., I. P. Sugar, and P. L. Chong. 2007. Critical factors for detection of biphasic changes in membrane properties at specific sterol mole fractions for maximal superlattice formation. *J. Phys. Chem. B.* **111:** 5180–5192.
44. Chiu, S. W., S. Vasudevan, E. Jakobsson, R. J. Mashl, and H. L. Scott. 2003. Structure of sphingomyelin bilayers: a simulation study. *Biophys. J.* **85:** 3624–3635.
45. Niemela, P., M. T. Hyvonen, and I. Vattulainen. 2004. Structure and dynamics of sphingomyelin bilayer: insight gained through systematic comparison to phosphatidylcholine. *Biophys. J.* **87:** 2976–2989.
46. Clarke, J. A., A. J. Heron, J. M. Seddon, and R. V. Law. 2006. The diversity of the liquid ordered (Lo) phase of phosphatidylcholine/cholesterol membranes: a variable temperature multinuclear solid-state NMR and x-ray diffraction study. *Biophys. J.* **90:** 2383–2393.
47. Korlach, J., P. Schwille, W. W. Webb, and G. W. Feigenson. 1999. Characterization of lipid bilayer phases by confocal microscopy and fluorescence correlation spectroscopy. *Proc. Natl. Acad. Sci. USA.* **96:** 8461–8466.
48. Wagner, A. J., S. Loew, and S. May. 2007. Influence of monolayer-monolayer coupling on the phase behavior of a fluid lipid bilayer. *Biophys. J.* **93:** 4268–4277.
49. Eisinger, J., and J. Flores. 1982. The relative locations of intramembrane fluorescent probes and of the cytosol hemoglobin in erythrocytes, studied by transverse resonance energy transfer. *Biophys. J.* **37:** 6–7.
50. Plasek, J., D. Cermakova, and P. Jarolim. 1988. Fluidity of intact erythrocyte membranes. Correction for fluorescence energy transfer from diphenylhexatriene to hemoglobin. *Biochim. Biophys. Acta.* **941:** 119–122.
51. Steck, T. L., J. Ye, and Y. Lange. 2002. Probing red cell membrane cholesterol movement with cyclodextrin. *Biophys. J.* **83:** 2118–2125.
52. Ohtani, Y., T. Irie, K. Uekama, K. Fukunaga, and J. Pitha. 1989. Differential effects of alpha-, beta- and gamma-cyclodextrins on human erythrocytes. *Eur. J. Biochem.* **186:** 17–22.
53. Kilsdonk, E. P., P. G. Yancey, G. W. Stoudt, F. W. Bangerter, W. J. Johnson, M. C. Phillips, and G. H. Rothblat. 1995. Cellular cholesterol efflux mediated by cyclodextrins. *J. Biol. Chem.* **270:** 17250–17256.
54. Gottfried, E. L. 1967. Lipids of human leukocytes: relation to cell type. *J. Lipid Res.* **8:** 321–327.
55. Parmahamsa, M., K. R. Reddy, and N. Varadacharyulu. 2004. Changes in composition and properties of erythrocyte membrane in chronic alcoholics. *Alcohol Alcohol.* **39:** 110–112.